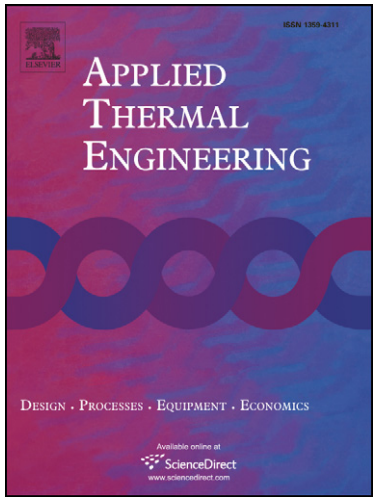

Measurements of brake disc surface temperature and emissivity by two-color pyrometry

Thevenet Jean, Siroux Monica, Desmet Bernard

PII: S1359-4311(09)00352-4
DOI: 10.1016/j.applthermaleng.2009.12.005
Reference: ATE 2942

To appear in: *Applied Thermal Engineering*

Received Date: 28 April 2009
Accepted Date: 9 December 2009

Please cite this article as: T. Jean, S. Monica, D. Bernard, Measurements of brake disc surface temperature and emissivity by two-color pyrometry, *Applied Thermal Engineering* (2009), doi: 10.1016/j.applthermaleng.2009.12.005

Measurements of brake disc surface temperature and emissivity by two-color pyrometry

Thevenet Jean[1,2], Siroux Monica[1,2]*, Desmet Bernard[1,2]

1 Univ Lille Nord de France, F-59000 Lille, France
2 UVHC, LME, F-59313 Valenciennes, France.
*Corresponding author. Tel: (33) 3 27 51 19 88, Fax: (33) 3 27 51 19 61
E-mail: Monica.Siroux@univ-valenciennes.fr

Abstract

A fiber optic two-color pyrometer was developed for brake disc surface temperature and emissivity measurements. The two-color pyrometer consists of a fluoride glass optical fiber, two HgCdTe detectors equipped with bandwidth filters and a data conditioning and acquisition device. The two-color pyrometer measures the brake disc temperature in the 200-800°C range with a time resolution of 8 µs. The calibration formula for the signals obtained using a blackbody of known temperature is used to compute the true temperature. The uncertainty estimation for temperature and emissivity was obtained from the calibration results. Tests were carried out on known temperature target and a good correlation was found between results obtained with our two-color pyrometer and those obtained with a commercial two-color pyrometer. Hold braking and deceleration braking tests performed on a braking test bench enabled us to reach the brake disc surface temperature and emissivity during braking. Experimental results show a significant variation of emissivity during braking. Direct measurement of emissivity was carried out on the brake disc after braking and shows the emissivity dependence with the surface quality.

Keywords: two-color pyrometer, brake disc, temperature, emissivity

Nomenclature

A	amplification constant, $V.W^{-1}.m^{3}.sr$
C	torque, $N.m$
C_1	first Planck constant, $W.m^{2}.sr^{-1}$
C_2	second Planck constant, $m.K$
d	spot diameter, m
h	distance, m
K	uncertainty coefficient
K_{CR}	grey body behavior assumption error coefficient
L	luminance, $W.m^{-3}.sr^{-1}$
p	pressure, Pa
R	ratio between reflected and emitted flux
S	detector signal, V
T	temperature, K

Greek symbols

ε	emissivity
λ	wavelength, μm
σ	relative value of the detector signal, V
τ	transmittivity
ω	rotational speed, rpm

Subscripts

λ_1	detector 1 of the two-color pyrometer
λ_2	detector 2 of the two-color pyrometer
λ_1/λ_2	fiber optic two-color pyrometer
bich	Impac™ two-color pyrometer
disc	brake disc
env	environment
pyro	Impac™ monochromatic pyrometer
ref	ambient signal

1 Introduction

Heat generated by the pad-disc contact during braking is the main cause of surface degradations such as oxidation, wear and thermo-mechanical failure, in particular, cracking [1]. In order to predict the consequences of thermal damage, several techniques have been developed to measure the temperature of sliding mechanical components: thermocouples techniques such as embedded thermocouples and dynamic thermocouples [2, 3, 4] and infrared techniques: pyrometry [5] and thermography [6].

Concerning optical temperature measurements during braking, some difficulties must be overcame: reduced size of the hot spots (about some millimeters during a high speed train emergency braking), fast phenomena [7] (some hot spots can have an observation time under 1 ms), difficulty of access. On the other hand, radiometric techniques need the knowledge of the brake disc emissivity [8]. This parameter depends on various factors, often time varying and depending of parameters such as the object temperature and its surface quality [9-12]. The bispectral or multispectral pyrometry can be a possible solution to overcome these difficulties: the radiometric measurements are simultaneously performed for two or more spectral ranges, allowing at the same time both the emissivity and temperature determination. Many authors have developed two-color or multi-color pyrometers with or without optical fiber [13-20]. Others authors have used infrared cameras to determine thermal mapping by monochromatic or multichromatic methods [21-25]. The bibliographical study shows that increasing the number of wavelengths does not necessarily imply a better accuracy on the temperature and need an adequate emissivity model to avoid a possible divergence of the temperature evaluation [10, 12, 14]. Moreover, in using a multispectral method, one has

to employ several detectors or several optical filters, which complicates the design and increases the cost of the apparatus.

The problematic is more complex in the case of braking given that the disc-rubbing surface evolves constantly during the test [26-29]. On the basis of this context, of the specific problems involved in the brake disc surface temperature measurement and while taking account the cost of the apparatus, a fiber optic two-color pyrometer was developed, able to make temperature and emissivity measurement of a brake disc. The pyrometer is composed of two HgCdTe detectors equipped with two bandwidth filters, a fluoride glass optical fiber and data conditioning and acquisition device. The fiber optic two-color pyrometer allows the brake disc surface temperature and emissivity measurements in the 200-800 °C range with a time response of 8 µs and a small measurement spot (2.4 mm).

2 Principle of the method

The theory of the two-color pyrometry is given in several references [10, 12, 14]. This method uses the Wien approximation of Planck's law [12, 13, 14, 30, 31] to determine the monochromatic luminance:

$$L_\lambda(\lambda,T) = \varepsilon_\lambda C_1 \lambda^{-5} \exp\left(-C_2 \big/ \lambda T\right) \tag{1}$$

with $C_1 = 1.19\times10^{-16}$ W.m^2.sr^{-1} and $C_2 = 1.44\times10^{-2}$ K.m.

The two-color pyrometry method measures the infrared luminance at two different wavelengths λ_1 and λ_2. In practice, the measurement signal is a voltage directly proportional to the luminance observed by the detectors:

$$\begin{aligned} S_{\lambda_1} &= A_{\lambda_1} L_{\lambda_1} = A_{\lambda_1} \varepsilon_{\lambda_1} C_1 \lambda_1^{-5} \exp\left(-C_2 \big/ \lambda_1 T\right) \\ S_{\lambda_2} &= A_{\lambda_2} L_{\lambda_2} = A_{\lambda_2} \varepsilon_{\lambda_2} C_1 \lambda_2^{-5} \exp\left(-C_2 \big/ \lambda_2 T\right) \end{aligned} \tag{2}$$

where A_{λ_1}, A_{λ_2} amplification constant of each detector.

The measurement signals are functions of the temperature and the emissivity of the surface. Assuming that the emissivity remains constant between λ_1 and λ_2 (grey body behavior) the temperature and the emissivity are obtained from the wavelength outputs S_{λ_1} and S_{λ_2}. The target temperature is obtained from the signal ratio $S_{\lambda_1} / S_{\lambda 2}$:

$$T = \frac{C_2\left(\frac{1}{\lambda_2} - \frac{1}{\lambda_1}\right)}{\ln\left(\frac{S_{\lambda_1}}{S_{\lambda_2}}\frac{A_{\lambda_2}}{A_{\lambda_1}}\left(\frac{\lambda_1}{\lambda_2}\right)^5\right)} \tag{3}$$

Consequently, the surface emissivity is expressed by substitution of T in S_{λ_1} or S_{λ_2} :

$$\varepsilon = \frac{\frac{S_{\lambda_i}}{A_{\lambda_i}}}{C_1\lambda_i^{-5}\exp\left(-C_2/\lambda_i T\right)} \qquad \text{i=1 or 2} \tag{4}$$

The temperature uncertainty is given by the total differential method [32]:

$$\frac{\Delta T}{T} = K\left(\frac{\Delta S_{\lambda_1}}{S_{\lambda_1}} + \frac{\Delta S_{\lambda_2}}{S_{\lambda_2}}\right) \tag{5}$$

where $\Delta S_{\lambda_i} / S_{\lambda_i}$ is the relative uncertainty on the wavelengths outputs and K an uncertainty coefficient which depends on λ_1, λ_2, T and C_2 [32]:

$$K = \left|\frac{T\lambda_1\lambda_2}{C_2(\lambda_2 - \lambda_1)}\right| \tag{6}$$

Increasing the separation of the wavelengths $\Delta\lambda=\lambda_1-\lambda_2$ reduces the temperature measurement uncertainty but the assumption of the grey body behavior can be less valid for large value $\Delta\lambda$. Therefore the choice of the two work wavelengths is a compromise between the grey body assumption, the temperature measurement uncertainty and the choice of equipment material [12, 19, 32]. For T = 1000 °C (which represents hot spots

temperature on a TGV brake disc during an emergency braking), the curves of constant value of K are drawn in the space λ_1, λ_2 (Figure 1). Taking into account the temperature measurement uncertainty, the grey body assumption and the filters availability, the wavelengths chosen in this study are λ_1 = 2.55 µm and λ_2 = 3.9 µm. These values are satisfactory to insure a sufficiently small wavelength separation and a reasonable effect on measurement uncertainty (K = 1.31).

To estimate the error corresponding to the grey body behavior assumption, an error coefficient K_{CR} can be defined from the difference between the measured temperature T_1 and the real surface temperature T_2 [32]:

$$\frac{T_2 - T_1}{T_1} = \frac{T_2 \ln\left(\frac{\varepsilon_{\lambda_1}}{\varepsilon_{\lambda_2}}\right)}{C_2\left(\frac{1}{\lambda_1} - \frac{1}{\lambda_2}\right)} = K_{CR} \tag{7}$$

The coefficient K_{CR} is a factor representative of the measurement error due to the grey body behavior assumption. The value of K_{CR} estimated for the two wavelengths previously chosen and taking into account the variations of the brake disc materials (steel, cast iron) emissivities given [33] is within 5%.

3 Experimental device

3.1 The two-color pyrometer

The portable two-color pyrometer shown in Figure 2, consists of a flexible fluoride glass optical fiber, two HgCdTe detectors equipped with bandwidth filters (Table 1) and a data conditioning and acquisition device. The optical fiber is mounted inside a flexible black tube in order to reduce reflections. The fluoride glass fiber has a high transmittivity, above 0.85 for the spectral range 0.5 - 4 µm [34]. The optical fiber attenuation is 0.3 dB/m for 4 µm. The core and clad diameter are 450 and 500 µm,

respectively and the numerical aperture of the fiber is 0.2. The two detectors are mounted on a three-stage Peltier cooling element, to reduce the detector noise. The time response of the HgCdTe detector is shorter than 2 µs. However, the detector signal is amplified by HgCdTe preamplifier. The preamplifier consists of two stages. The first stage is a transresistance amplifier equipped with a bias and offset supply. The second stage is an inverting gain amplifier. Therefore the preamplifier is inverting and supplies a decreasing signal when the detector is exposed to radiation. The bandwidth of the preamplifier is 0-150 kHz and consequently the time response of the detection system is about 8 µs. The detectors equipped with bandwidth filters and the data conditioning and acquisition device are mounted in an enclosure to isolate the detectors from the environment. This enclosure is ventilated to avoid the heating of the different components.

The measured spot diameter, noted *d*, is a function of the distance between the fiber and the target, noted *h*. An experiment was carried out to verify this theoretical value. A source of visible light was used to visualize the spot of the optical fiber, and a graph paper gave the measurement of the spot diameter. The experimental and theoretical data are very close. The use of the optical fiber gives small measurement spots. For example, if the distance between the fiber extremity and the brake disc surface is 5 mm the spot diameter is about 2.4 mm.

3.2 Calibration procedure

The calibration procedure, which is very important for the temperature evaluation, consisted in heating a blackbody and obtaining the calibration curve of each detector. The two-color pyrometer was calibrated using an extended blackbody HGH (type ECN 100 H6, emissivity $\varepsilon = 0.98 \pm 0.02$, temperature range 50 - 550 °C, absolute error

temperature ΔT = ± 0.5 °C). The temperature of the blackbody was varied from 200 to 550°C by steps of 50°C. For each temperature, 10 acquisitions were made with the two-color pyrometer. The target is alternatively the extended blackbody (blackbody signal) and the environment at ambient temperature (ambient signal).

From the calibration, it appears that for a given ambient temperature there is a drift of the signal. A recording of the ambient signal and blackbody signal was made and the evolution of the ambient signal was confirmed. However, the signal drift during braking test (about 150 s) is too weak to influence the measurement. It was also observed that the difference between the blackbody signal and the reference signal remained constant, so a relative value was used:

$$\sigma_{\lambda_i} = S_{\lambda_i,réf} - S_{\lambda_i} \tag{8}$$

For each point of calibration, $S_{\lambda_i,réf}$ is the average of the ambient signal and S_{λ_i} is the average of the blackbody signal. So for each temperature and each luminance, 10 values of σ_{λ_i} can be obtained and consequently the calibration curves $\sigma = f(L)$ are easily obtained.

Some tests were carried out for temperature lower than 200°C to verify the sensor thresholds. For these temperatures, the signals from the detectors did not vary. During the calibration, the temperature of the ambient source is lower than the sensor threshold so the ambient signal can be used as the reference signal.

The detector noise is evaluated using a spectrum analysis. Both blackbody and environment are used as source and gives two similar spectrums. The noise of the detector has a wide band spectrum. Because the signal to noise ratio is about 200 at 400°C, the detector noise contribution is not significant.

Figure 3 shows the proportionality between the luminance and the output signal. The radiances are calculated for the spectral bands of the detectors. The two amplification constants are determined using calibration curves:

$$A_{\lambda_1} = 2.39\times10^{-9}\ \mathrm{V.W^{-1}.m^3.sr};\ A_{\lambda_2} = 3.16\times10^{-10}\ \mathrm{V.W^{-1}.m^3.sr} \quad (9)$$

3.3 Influence of the surrounding radiation on measurements

The influence of the surrounding radiation [13, 35, 36] on measurement results has been studied. The two-color pyrometer received both emitted and reflected flux. The total luminance incoming from the sample is:

$$L_\lambda = \varepsilon_\lambda C_1\,\lambda^{-5}\exp\left(-\frac{C_2}{\lambda T}\right)+\left(1-\varepsilon_\lambda\right)C_1\,\lambda^{-5}\exp\left(-\frac{C_2}{\lambda T_{env}}\right) \quad (10)$$

where T is the surface temperature of the object and T_{env} the surrounding temperature.

During the braking tests the disc surface temperature is higher than 400°C, the environment temperature is about 20°C, the optical fiber is placed close to the pad-disc contact using a black mounting bracket held near room temperature. At temperature higher than 300°C the ratio between reflected and emitted flux estimated using equation (10) is about 0.004, so the reflected flux can be neglected.

3.4 *Uncertainty analysis*

The temperature and emissivity uncertainties can be obtained using the Law of Propagation of Uncertainty [37, 38, 39, 40, 41]:

$$\begin{aligned}\Delta T^2 = &\left(\frac{\partial T}{\partial \sigma_{\lambda_1}}\right)^2\left(\Delta\sigma_{\lambda_1}\right)^2+\left(\frac{\partial T}{\partial \sigma_{\lambda_2}}\right)^2\left(\Delta\sigma_{\lambda_2}\right)^2+\left(\frac{\partial T}{\partial A_{\lambda_1}}\right)^2\left(\Delta A_{\lambda_1}\right)^2+\left(\frac{\partial T}{\partial A_{\lambda_2}}\right)^2\left(\Delta A_{\lambda_2}\right)^2\\ &+\left(\frac{\partial T}{\partial \lambda_1}\right)^2\left(\Delta\lambda_1\right)^2+\left(\frac{\partial T}{\partial \lambda_2}\right)^2\left(\Delta\lambda_2\right)^2+2\frac{\partial T}{\partial \sigma_{\lambda_1}}\frac{\partial T}{\partial \sigma_{\lambda_2}}\mathrm{cov}\left(\sigma_{\lambda_1},\sigma_{\lambda_2}\right)\end{aligned} \quad (11)$$

$$\Delta\varepsilon^2 = \left(\frac{\partial\varepsilon}{\partial\sigma_{\lambda_i}}\right)^2 \left(\Delta\sigma_{\lambda_i}\right)^2 + \left(\frac{\partial\varepsilon}{\partial A_{\lambda_i}}\right)^2 \left(\Delta A_{\lambda_i}\right)^2 + \left(\frac{\partial\varepsilon}{\partial\lambda_i}\right)^2 \left(\Delta\lambda_i\right)^2 + \left(\frac{\partial\varepsilon}{\partial T}\right)^2 \left(\Delta T\right)^2 \quad (12)$$

Where $\Delta\sigma_{\lambda_1}$ and $\Delta\sigma_{\lambda_2}$ are the signals variances, ΔA_{λ_1} and ΔA_{λ_2} are the amplification constants variances, $\Delta\lambda_1$ and $\Delta\lambda_2$ the wavelength variances and $\mathrm{cov}\left(\sigma_{\lambda_1}, \sigma_{\lambda_2}\right)$ is the signals covariance. Using equations (11) and (12) the relative uncertainties of the temperature and the emissivity can be determined:

$$\frac{\Delta T}{T} = K\sqrt{\left(\frac{\Delta\sigma_{\lambda_1}}{\sigma_{\lambda_1}}\right)^2 + \left(\frac{\Delta\sigma_{\lambda_2}}{\sigma_{\lambda_2}}\right)^2 + \left(\frac{\Delta A_{\lambda_1}}{A_{\lambda_1}}\right)^2 + \left(\frac{\Delta A_{\lambda_2}}{A_{\lambda_2}}\right)^2 - 2\frac{\mathrm{cov}\left(\sigma_{\lambda_1}, \sigma_{\lambda_2}\right)}{\sigma_{\lambda_1}\sigma_{\lambda_2}} + \left(5 - \frac{C_2}{\lambda_1 T}\right)^2 \left(\frac{\Delta\lambda_1}{\lambda_1}\right)^2 + \left(5 - \frac{C_2}{\lambda_2 T}\right)^2 \left(\frac{\Delta\lambda_2}{\lambda_2}\right)^2} \quad (13)$$

$$\frac{\Delta\varepsilon}{\varepsilon} = \sqrt{\left(\frac{\Delta\sigma_{\lambda_i}}{\sigma_{\lambda_i}}\right)^2 + \left(\frac{C_2}{\lambda_i}\right)^2 \left(\frac{\Delta T}{T}\right)^2 + \left(\frac{C_2}{\lambda_i T} - 5\right)^2 \left(\frac{\Delta\lambda_i}{\lambda_i}\right)^2 + \left(\frac{\Delta A_{\lambda_i}}{A_{\lambda_i}}\right)^2} \quad (14)$$

In equations (13) and (14) the estimated uncertainty of the central wavelength $\frac{\Delta\lambda_i}{\lambda_i}$ is 1 % according to the manufacturer specification.

The curve $\Delta T = f\left(T\right)$ is presented in the Figure 4, for temperatures higher than 300°C, the temperature uncertainty is lower than 18 °C.

The curve $\Delta\varepsilon = f\left(T\right)$ is presented in the Figure 4, the emissivity uncertainty remains lower than 0.21 and 0.15 for temperatures higher than 300°C and 350°C respectively.

3.5 Experimental validation

To validate the two-color pyrometer, tests were carried out on a disc covered with a known emissivity black paint (ε = 0.93±0.02) [42]. The surface temperature was measured simultaneously by our new two-color pyrometer ($T_{\lambda 1/\lambda 2}$) and a commercially available Impac™ two-color pyrometer (T_{bichro}) (pyrometer reference IGAR 12 LO,

temperature range 300-1000°C, measurement wavelengths: 1.52 μm and 1.64 μm). The temperatures obtained with the two pyrometers are almost identical. The average deviation between the temperatures recorded by the two pyrometers is about 2 °C and remains lower than the two-color pyrometer uncertainty who is about 14 °C. These tests enabled us to validate the method of measurement.

4 Braking test bench experimental results

Experiments were carried out on a SCHENCK braking test bench at the C3T (Ground Transportation Technological Centre) (Figure 5). This test bench is composed of four parts: the test cell, the drive system, flywheels and the base. The test cell is an enclosure ensuring a control of the room temperature and allowing a correct ventilation of the disc. The enclosure is equipped with two port-holes for the radiometric measurements. One end of the driving shaft equipped with a rotary transmitter is in the test cell. The drive system is a DC machine. The flywheels and the drive system are used to simulate the brake inertia.

The brake system is composed of a 259 mm diameter ventilated disc equipped with 2 K-type thermocouples placed at the friction radius 6 mm under the disc surface and two pads (pad surface: 30 cm^2) equipped with 2 K-type thermocouples placed 5 mm under the contact surface (Figure 6). The optical fiber of the two-color pyrometer is placed close to the pad-disc contact using a black mounting bracket which was held near room temperature in order to avoid reflections on the brake disc surface. The distance between the fiber and the surface disc is 5 mm. According to the characteristics of the optical fiber, the spot diameter is 2.4 mm. To control the measurement of the two-color pyrometer, the disc surface temperature is also measured by a monochromatic Impac^{TM}

pyrometer (pyrometer reference IP 140, temperature range: 75 - 550°C, spectral range : 2 - 2.8 μm).

Two kinds of test were undertaken on the C3T test bench (Table 2):

- Deceleration braking: decreasing revolving speed
- Hold braking: braking with constant torque and constant rotational speed.

The sampling frequency is 100 Hz, in order to satisfy the sampling condition according to Shannon's theorem.

4.1 Deceleration braking

Figure 7 shows the brake disc temperature and emissivity evolution during deceleration braking test:

- $T_{\lambda 1/\lambda 2}$ is the surface temperature measured by the two-color pyrometer (ratio of the signal from each detector),
- $T_{\lambda 1}$ and $T_{\lambda 2}$ are the monochromatic surface temperatures measured by each detector of the two color pyrometer assuming a blackbody behavior for the disc surface ($\varepsilon = 1$),
- T_{pyro} is the temperature measured by the monochromatic pyrometer IMPAC^{TM} (IP 140), assuming a blackbody behavior for the disc surface ($\varepsilon = 1$),
- T_{disc} is the mass disc temperature measured by thermocouple 6 mm under the friction surface.
- ε is the emissivity of the surface measured by the two-color pyrometer

The temperature increases quickly at the beginning of the braking, the maximum temperature is reached after 20 s, and then it decreases. The monochromatic temperatures $T_{\lambda 1}$, $T_{\lambda 2}$ are similar to the monochromatic pyrometer IMPAC^{TM} temperature T_{pyro}. The monochromatic temperatures was measured by the monochromatic pyrometer IMPAC^{TM} (IP 140) and by each detector of our two-color

pyrometer assuming a blackbody behavior for the disc surface ($\varepsilon = 1$). The monochromatic temperatures ($T_{\lambda 1}$, $T_{\lambda 2}$, T_{pyro}) are so underestimated [12, 13]. A difference of around 150 °C between the monochromatic temperatures (assuming a blackbody behaviour for the disc surface) and the two-color temperature is observed. This difference can be explained by the brake disc emissivity evolution during the test. The brake disc emissivity increases with the temperature reduction (Figure 7). The emissivity value is 0.45 at the beginning of the braking, 0.4 for the maximum temperature and 0.7 at the end of the test. This increase of the emissivity with the reduction of the temperature is coherent with the bibliography [25, 26, 28, 29]. The variation of the emissivity is the consequence of the evolution of the properties of friction surface during braking.

4.2 Hold braking

Figure 8 shows the brake disc temperature and emissivity evolution during hold braking test. As it can be observed in Figure 8, the frequency of the temperature oscillations corresponds to the frequency of the disc rotation. It can be seen that the monochromatic temperatures $T_{\lambda 1}$ and $T_{\lambda 2}$ obtained from the two detectors are close to the monochromatic temperature measured by the IMPAC^{TM} monochromatic pyrometer T_{pyro}. However, a significant difference between the two-color temperature $T_{\lambda 1/\lambda 2}$ and the monochromatic temperatures $T_{\lambda 1}$, $T_{\lambda 2}$ and T_{pyro} is observed. Once again, this difference can be explained by the brake disc emissivity evolution during braking.

The emissivity is around 0.5 at the beginning of braking, decreases to around 0.35 for t = 20 s and increases to around 0.4 at the end of the braking sequence. The evolution of the emissivity over time can be explained by the temperature variation and the modification of the brake disc surface during braking. While the two-color temperature

value is about 500°C, the estimated temperature uncertainty is lower than 14 °C (Figure 4) and the estimated emissivity uncertainty is lower than 0.09 (Figure 4).

Direct measurements of emissivity were carried out on the brake disc after braking. The disc was heated at 550 °C and a part of the heated disc was covered with a known emissivity black paint ($\varepsilon = 0.93 \pm 0.02$). The surface temperature was measured with an infrared camera (CEDIP, λ = 3-5 μm) and the two-color pyrometer. The disc emissivity is determined using the ratio of the disc and the black paint luminance. Figure 9 shows brake disc emissivity values obtained during braking using the two-color pyrometer and brake disc emissivity obtained after braking using the infrared camera and the two-color pyrometer. As it can be seen in Figure 9, a good correlation was found between pyrometer and infrared camera direct emissivity measurements. However, emissivity values obtained after braking using the direct method are higher (about 0.8) than emissivity values obtained during braking (about 0.4). This difference can be explained by the oxidation of the disc surface observed after braking. This corresponds to the bibliographical study [33] which shows that the emissivity at T = 600 °C and for λ between 2.5 and 5 μm, varies between 0.35 and 0.2 for bright metals and between 0.7 and 0.9 for oxidized metals.

5 Conclusion

A fiber optic two-color pyrometer with a short time response (8 μs) and a small measurement spot (2.4 mm) capable of measuring the brake disc surface temperature and emissivity in the 200-800°C range has been developed. The two-color device consists of a fluoride glass fiber, two HgCdTe detectors equipped with bandwidth filters and a data conditioning and acquisition device. The two-color pyrometer was calibrated using an extended blackbody. Tests were carried out on known temperature target and a

good correlation was found between results obtained with our two-color pyrometer and those obtained with a commercial two-color pyrometer. Some experiments carried out on a braking test bench enabled us to reach the transient brake disc surface temperature during braking and proved the importance of the emissivity on the measurement of the disc surface temperature. A significant variation of the emissivity has been observed for both hold braking and deceleration braking. Direct measurement of emissivity carried out on the brake disc after braking shows the emissivity dependence with the surface oxidation. Further, the two-color pyrometer can be used to investigate the temperature effect on the tribological behaviour of the brake disc during braking.

Acknowledgments

The authors would like to thank the European Community and the Région Nord – Pas de Calais for the financial support given to the present study.

References

[1] A-L. Cristol-Bulthé, Y. Desplanques, G. Degallaix, Y. Berthier, Mechanical and chemical investigation of the temperature influence on the tribological mechanisms occurring in OMC/cast iron friction contact, Wear 264 (2008) 815-825.

[2] F. Kennedy, D. Frusescu, J. Li, Thin film thermocouple arrays for sliding surface temperature measurement, Wear 207 (1997) 46-57.

[3] P. Dufrenoy, Etude du comportement thermomécanique des disques de frein vis à vis des risques de défaillance. Application au domaine ferroviaire, Thèse de doctorat, Université de Lille, 1995.

[4] J. Denape, N. Laraqi, Aspect thermique du frottement : mise en évidence expérimentale et éléments de modélisation, Mécanique & Industries 1 (2000) 563-579.

[5] M Siroux, A-L. Bulthe, Y. Desplanques, B. Desmet, G. Degallaix, Thermal analysis of periodic sliding contact on a braking tribometer, Applied Thermal Engineering 28 (2008) 2194-2202.

[6] D. Majcherczak, P. Dufrenoy, Y. Berthier, Tribological, thermal and mechanical coupling aspects of the dry sliding contact, Tribology International 40 (2007) 834-843 .

[7] F. Benillouche, D. Pajani, P. Bremond, P. Potet, Thermographie infrarouge d'objets tournant à grande vitesse, Ingénieurs de l'automobile 667 (1992) 51-53.

[8] S. Matteï, Traité Génie Énergétique Rayonnement thermique des matériaux opaques, Techniques de l'Ingénieur, BE 8 210, 1-24, 2005.

[9] P. Hervé, Mesure de l'émissivité thermique, Techniques de l'ingénieur R 2737, 2005.

[10] J. Hladik, Métrologie des propriétés thermophysiques des matériaux, Masson, 1990.

[11] J.F. Sacadura, Measurement Techniques for Thermal Radiation Properties, Proc. 9th, Int. Heat Transfer Conf. Jerusalem 1, (1990) 207-222.

[12] F. Cabannes, Pyrométrie optique, Traité : Mesures et contrôle, Techniques de l'ingénieur R2610, 1990.

[13] F. Cabannes, Température de surface : Mesure radiative, Techniques de l'ingénieur R 2735, 1996.

[14] P. Ferdinand, Thermomètres à fibre optique sans contact, Techniques de l'ingénieur R 2801, 2003.

[15] R. Komanduri, Z.B. Hou., A review of the experimental techniques for the measurement of heat and temperatures generated in some manufacturing process and tribology, Tribology International 34 (2001) 653-682.

[16] T Ueda, M. Sato, T. Sugita, K. Nakayama, Thermal Behaviour of Cutting Grain in Grinding, Annals of the CIRP44 (1995) 325-328.

[17] T. Ueda, K. Yamada, K. Nakayama, Temperature of Work materials irradiated with CO_2 laser, Annals of the CIRP 46 (1997) 117-122.

[18] H. Zhao, N. Ladammatos, Optical Diagnostics for soot and temperature measurement in diesel engines, Prog Enery Combust Sci 24 (1998) 221-255.

[19] B. Müller, U. Renz, Time resolved temperature measurements in manufacturing, Measurements 34 (2003) 363-370.

[20] Y. Tago, F. Akimoto, K. Kitaga, N. Arai, Spectoscopic Measurements of High Emissivity Materials Using Two-Dimensional Two-Color Thermometry, Transaction of ASME 127 (2005) 472-477.

[21] T. Inagaki, T. Ishii, Proposal of quantitative temperature measurement using two-color technique combined with several infrared radiometers having different detection wavelength bands, Optical Engineering 40 (3) (2001) 372-380.

[22] Legrand, Thermographie multispectrale haute et basse température. Application au contrôle non destructif, Thèse de l'Université Bourgogne, 2002.

[23] L. Viellard, P. Herve, L. Azizi, H. Bouaert, Mesure simultanée de la température et de l'émissivité sur un four industriel de recuit en continu, Congres SFT (1996), 84-89.

[24] T. Inagaki, T. Ishii, On the proposal of quantitative temperature measurement by using three-color technique combined with several infrared sensors having different detection wavelength bands, Infrared Physics &Technology 41 (2000) 205-237.

[25] Y. Tago, F. Akimoto, K. Kitaga, N. Arai, Spectroscopic Measurements of surface temperature and emissivity by two-dimensional four-color thermometry with narrow band, Energy (2005) 485-495.

[26] D. Pajani, P. Bremond, Thermographie infrarouge, Techniques de l'ingénieur R 2740, 2001.

[27] S. Panier, P. Dufrenoy, W. Dieter, An experimental investigation of hot spots in railway disc brakes, Wear 256 (2004) 764-773.

[28] F. Cartigny, R. Copin, M. Siroux, S. Harmand, Y. Desplanques, G. Degallaix, B. Desmet, Cartographies d'émissivité de la surface d'un disque de frein, Congrès SFT Lyon (2000) 351-356.

[29] B. Desmet, M. Siroux, F. Cartigny, S. Harmand, Y. Desplanques, G. Degallaix, Métrologie thermique du contact en freinage, European Conference on braking JEF Lille (2002) 369-376.

[30] T. Borca-Tasciuc, G. Chen, Temperature measurement of fine wires by photothermal radiometry, Rev. Sci. Instrument. 68 (1) (1997) 4080-4083.

[31] J.F. Sacadura, Initiations aux transferts thermiques, Technique et Documentation, 1999.

[32] S. Lefèvre, Métrologie thermique adaptée à un dispositif de freinage ferroviaire, Rapport de Post Doctorat, Université de Valenciennes, 2006.

[33] W. Bauer, H. Oertel, M. Rink, Spectral emissivity of bright and oxidized metals at high temperatures, Fifteen Symposium on thermophysical Properties, Boulder, Colorado (2003).

[34] Document technique, Le Verre Fluoré, 2006.

[35] T. Duvaut, D. Georgeault, J.L. Beaudoin, Multiwavelength infrared pyrometry: optimization and computer simulations, Infrared Physics & Technology 36 (1995) 1089-1103.

[36] Y. N'Guessan, Contribution à l'étude des propriétés radiatives des matériaux opaques ou semi-transparents, à température ambiante, par une méthode radiométrique en régime modulé, Thèse Université Paris XII, 1996.

[37] P. Coppa, A. Consorti, Normal emissivity of samples surrounded by surfaces at diverse temperatures, Measurement 38 (2005) 124-131.

[38] AFNOR, Norme NF ENV 13005 (X07-020), Guide pour l'expression de l'incertitude de mesure, 1999.

[39] M. Priel, Incertitudes de mesure et tolérances, Techniques de l'ingénieur R 285, 1999.

[40] B.N. Taylor, C.E. Kuyatt, Guidelines for Evaluating and Expressing the Uncertainty of NIST Measurement Results, NIST Technical Note 1297, 1994.

[41] M. Siroux, Habilitation à diriger des recherches, Université de Valenciennes, 2008.

[42] M. Siroux, S. Harmand, B. Desmet, Experimental study using infrared thermograhy on the convective heat transfer of a TGV brake disc in the actual environment, Optical Engineering 41 (7) (2002)1558-1564.

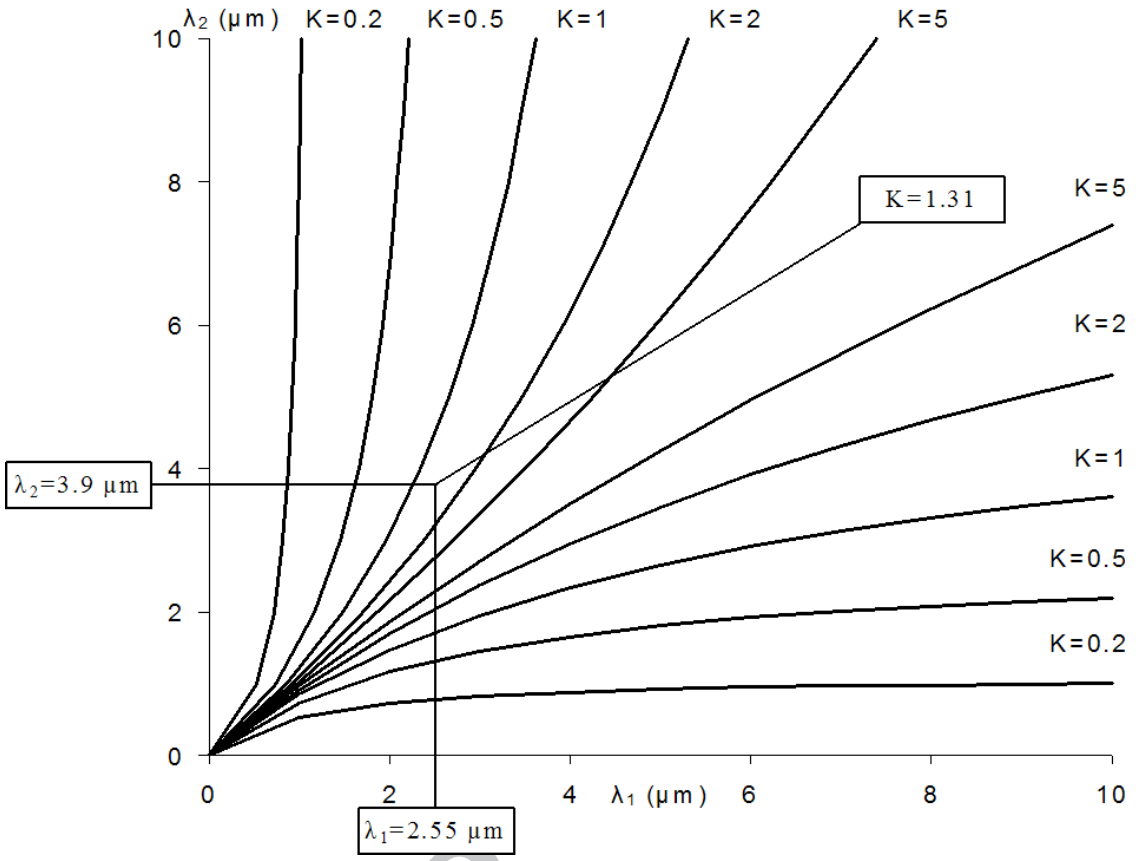

Figure.1. "Iso-K" curves in the space (λ_1,λ_2)

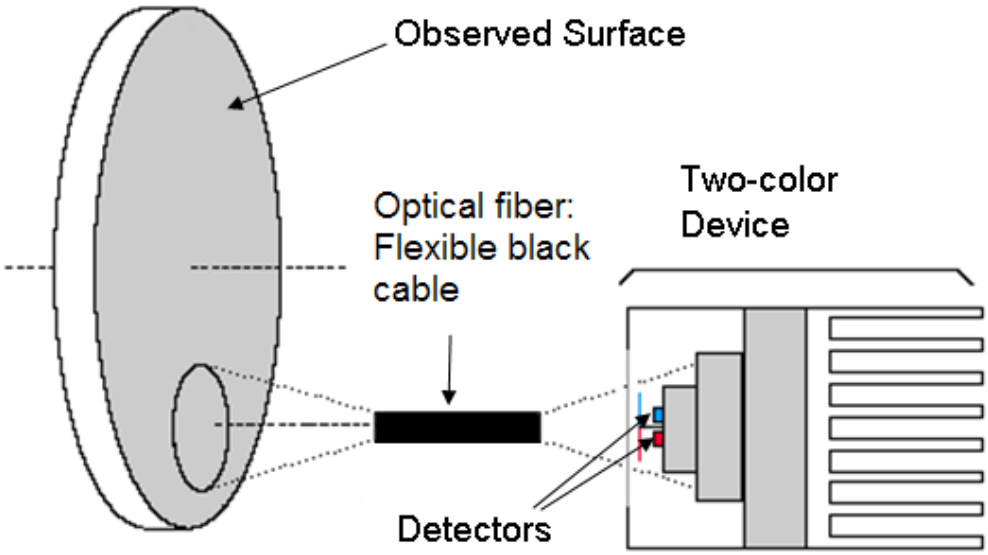

Figure.2. Experimental device

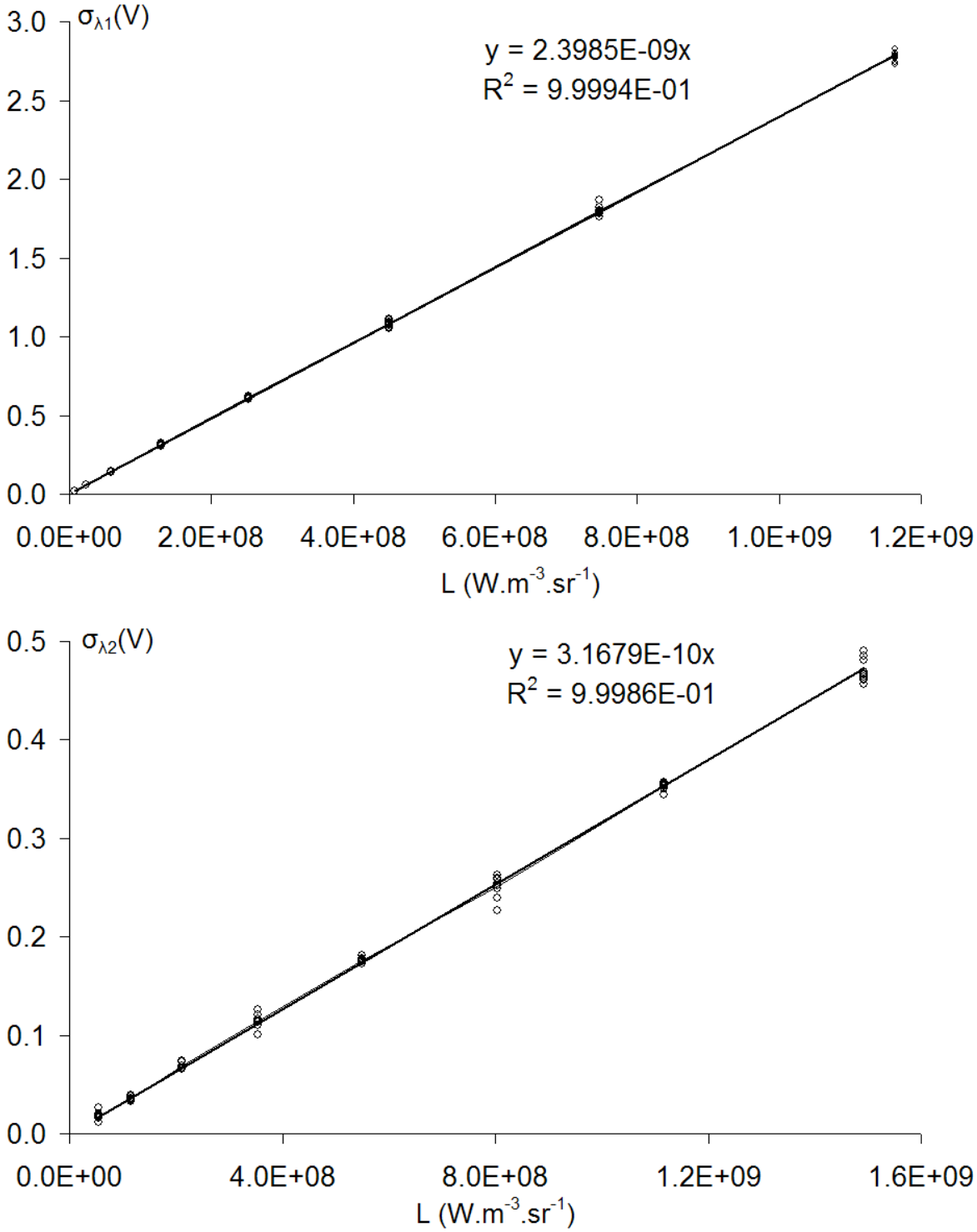

Figure.3. Calibration curves σ = f(L)

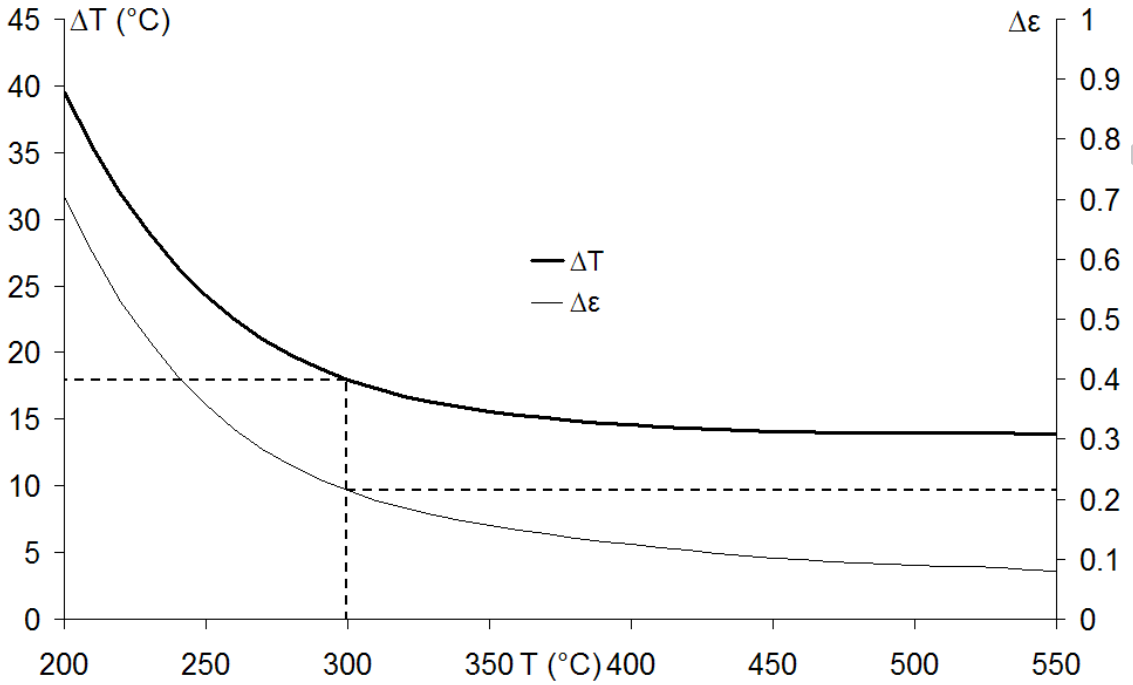

Figure.4. Temperature and emissivity uncertainties

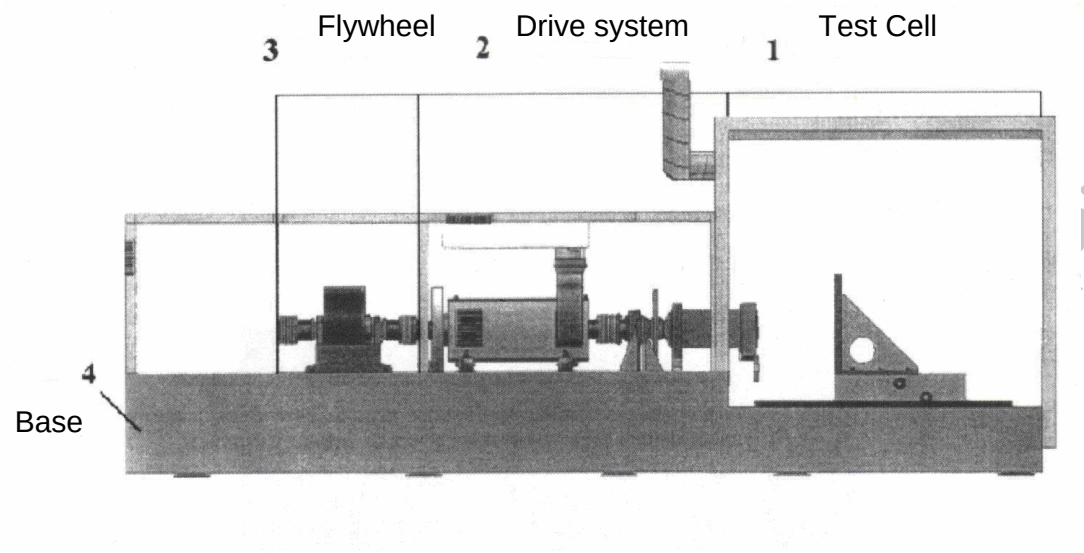

Figure.5. Representation of the test bench

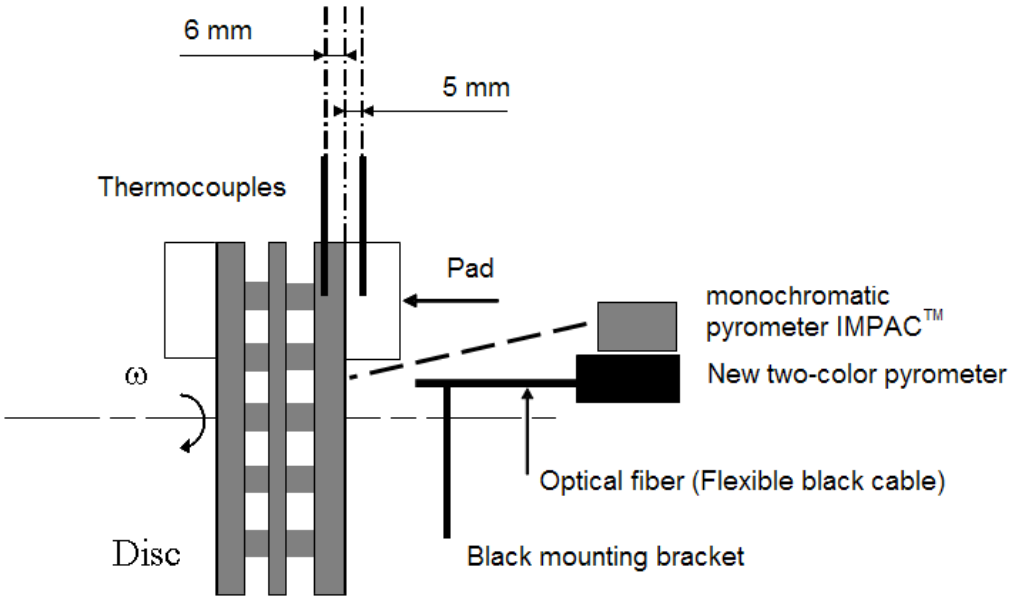

Figure.6. Brake disc and pin : Temperature measurements

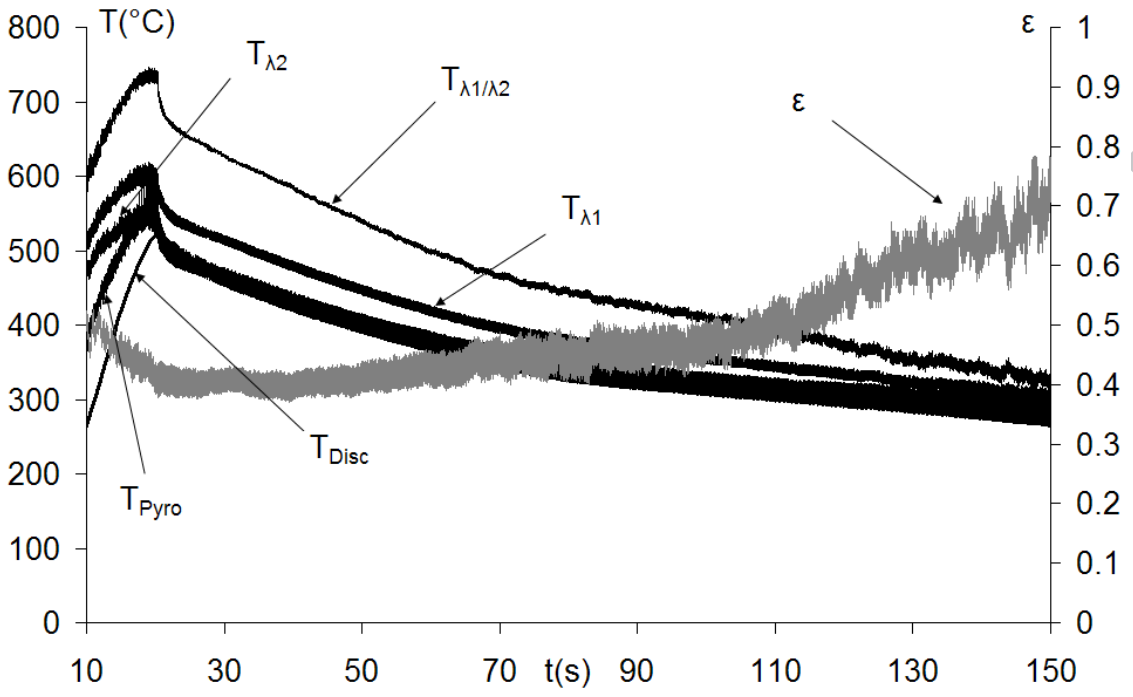

Figure.7. Brake disc temperature and emissivity evolution during deceleration braking

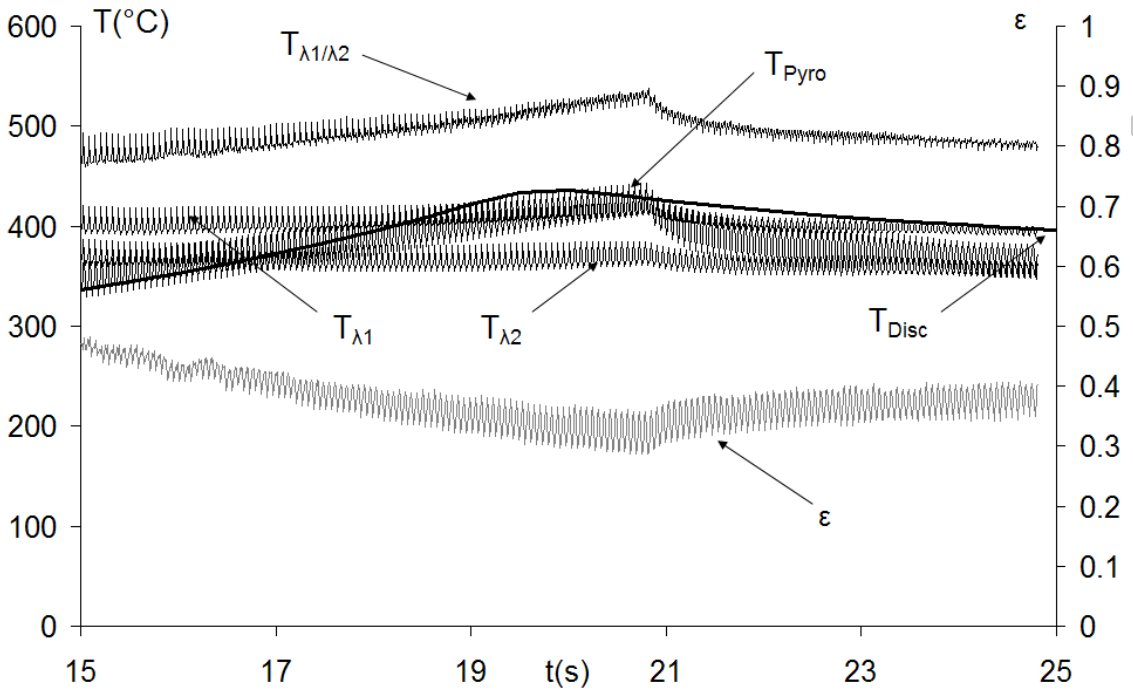

Figure.8. Brake disc temperature and emissivity evolution during hold braking

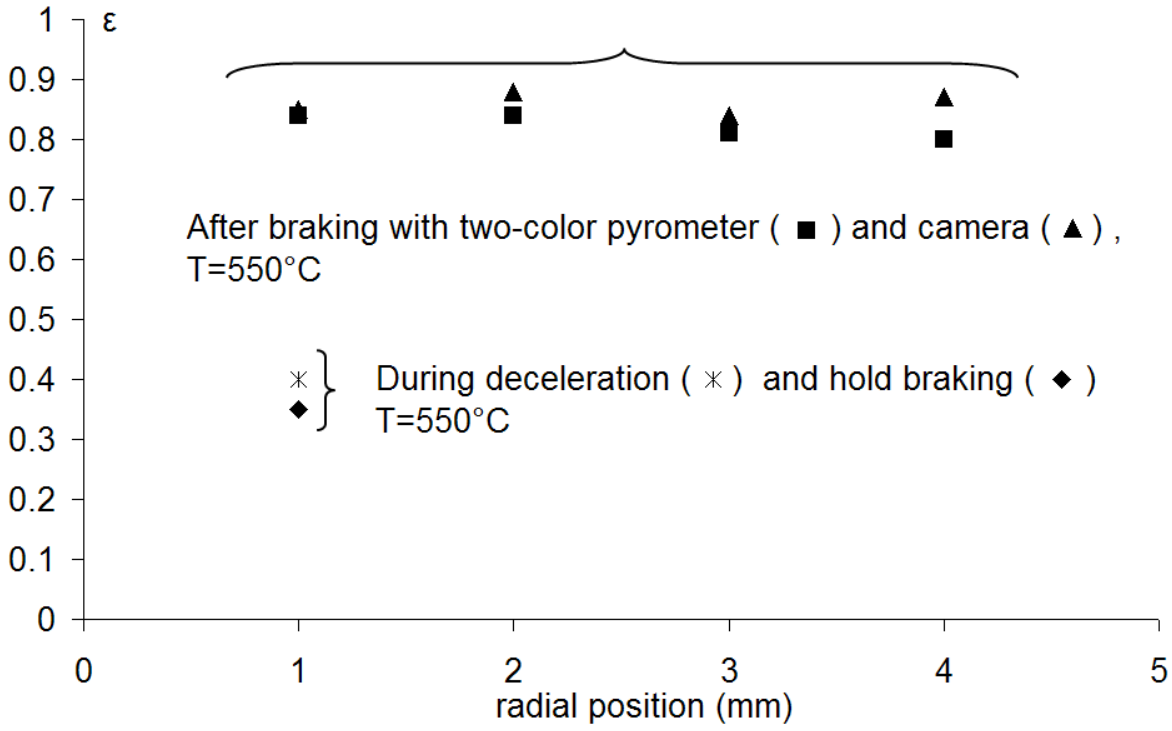

Figure.9. Brake disc emissivity

Optical Fiber	Fluoride Glass Spectral range: 0.5-4 μm Core/clad diameter: 450/500 μm Numerical aperture 0.2 Attenuation for 4 μm: 0.3 dB/m Length: 1m Transmittivity: 0.85
Detectors	Detector HgCdTe 1 mm x 1 mm Time response: < 2 μs
IR Filters	Bandwidth Filter Filter 1 central wavelength: 2.55 μm Filter 2 central wavelength: 3.9 μm Transmittivity: 0.7

Table.1. Characteristics of the two-color device components

Hold braking	Deceleration braking
ω = 1000 rpm $C_{braking}$ = 50 Nm $p_{braking}$ = 1.05 bar	ω = 1292 to 373 rpm $p_{braking}$ = 24.6 bar

Table.2. Characteristics of the test